Exp Brain Res (2001) 141:312–323
DOI 10.1007/s002210100880

RESEARCH ARTICLE

Eric J. Perreault · Robert F. Kirsch · Patrick E. Crago

Effects of voluntary force generation on the elastic components of endpoint stiffness

Received: 15 March 2001 / Accepted: 6 August 2001 / Published online: 11 October 2001

Abstract The goal of this work was to determine how force loads applied at the hand change the elastic mechanical properties of the arm. Endpoint stiffness, which characterizes the relationship between hand displacements and the forces required to effect those displacements, was estimated during the application of planar, stochastic displacement perturbations to the human arm. A nonparametric system identification algorithm was used to estimate endpoint stiffness from the measured force and displacement data. We found that changes in the elastic component of arm stiffness during isometric force regulation tasks were due primarily to the actions of the single-joint muscles spanning the shoulder and elbow. This was shown to result in a nearly posture-independent regulation of joint torque-stiffness relationships, suggesting a simplified strategy that is used to regulate arm mechanics during these tasks.

Keywords Biomechanics · Endpoint stiffness · Joint stiffness · Motor control · Multijoint · Posture

Introduction

The human arm presents a stable mechanical interface to its environment, allowing it to make reliable contact with a variety of objects and to maintain stable postures in the face of uncertain and often destabilizing loads. Understanding how the mechanical properties of the arm, specifically its stiffness, are modified during functional tasks may elucidate the underlying neuromotor control strategies. This study examined how the elastic components of endpoint stiffness are modulated by changes in voluntary effort during isometric force regulation tasks, where individuals exert voluntary forces against a rigid object. Our results suggest that, during such tasks, posture-dependent changes in endpoint stiffness result predominantly from changes in arm orientation, while the individual stiffness properties of the elbow and shoulder joints are regulated in a nearly posture-independent manner.

Endpoint stiffness, defined as the relationship between externally applied displacements of the hand and the forces generated in response, was used to characterize the arm mechanics. Such stiffness measurements are thought to be related closely to postural stability (Feldman 1966; Bizzi and Abend 1983; Hogan 1985; Colgate and Hogan 1988; Lacquaniti et al. 1993; Gomi and Osu 1998). The stiffness of the elbow and shoulder joint structures, the muscles acting about these joints, and the limb geometry all contribute to endpoint stiffness. For a given arm posture, endpoint stiffness properties can be modified by changes in muscle activation. Hogan (1985) first proposed that the central nervous system could maintain arm stability via regulation of its endpoint stiffness properties. Since then, numerous studies have examined the multijoint stiffness of the human arm. Mussa-Ivaldi et al. (1985) showed that the static endpoint stiffness properties are highly dependent upon arm posture. For most postures in the horizontal plane, the arm is stiffest for disturbances directed from the hand toward the center of rotation of the glenohumeral joint. Flash and Mussa-Ivaldi (1990) determined that this postural dependence was due not only to the changes in arm posture, but also to a posture-dependent regulation of the joint stiffnesses. These studies, though, were limited to conditions where the subject was at rest. Few studies have examined how the endpoint stiffness characteristics change when the arm also generates significant forces. The most complete study was performed by Gomi and Osu (1998), who found that both stiffness orientation and relative stiffness in different directions were depen-

E.J. Perreault (✉)
Department of Physiology, Ward 5-295,
Northwestern University Medical School, 303E. Chicago Ave.,
Chicago, IL 60611, USA
e-mail: e-perreault@northwestern.edu
Tel.: +1-312-5031323, Fax: +1-312-5035101

E.J. Perreault · R.F. Kirsch · P.E. Crago
Case Western Reserve University, Cleveland, OH, USA

E.J. Perreault · R.F. Kirsch · P.E. Crago
Louis Stokes VA Medical Center, Cleveland, OH, USA

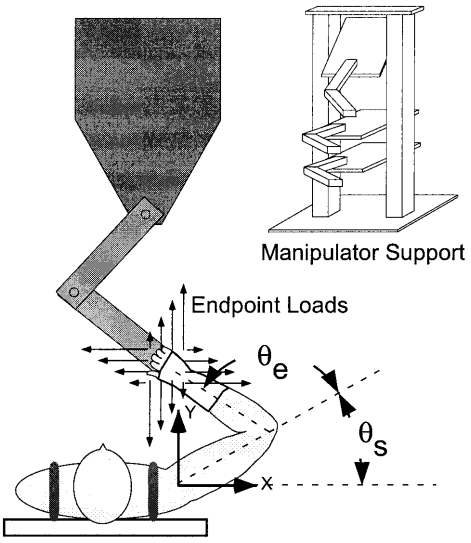

Fig. 1 Experimental setup. A two-joint robotic manipulator was used to apply endpoint perturbations in these experiments. The manipulator was mounted on an adjustable structure, allowing its height to be customized for each subject. During each trial, subjects exerted a constant force on the manipulator in one of the four directions shown. Force magnitudes ranged from 0% to 30% MVC

dent upon endpoint force properties during the voluntary generation of moderate endpoint forces.

In this study, we sought to extend the work of Gomi and Osu by examining changes in arm stiffness for significantly larger endpoint forces and by better examining the control strategies underlying the observed changes in endpoint stiffness. We found that changes in arm stiffness during isometric force regulation tasks were due primarily to the actions of the single-joint muscles spanning the shoulder and elbow. This was shown to result in a nearly posture-independent regulation of joint torque-stiffness relationships, suggesting a simplified strategy that is used to regulate arm mechanics during these tasks.

Materials and methods

Experimental

Apparatus

Endpoint stiffness was estimated using perturbations applied by a two-joint robotic manipulator described in detail previously (Acosta et al. 2000) and summarized briefly below. Figure 1 illustrates this device, which was configured as a position servo for these experiments. Subjects were strapped into a rigid chair with custom supports to constrain both lateral and anterior-posterior trunk movements. Each subject's arm was attached to the endpoint of the manipulator via a custom-fitted fiberglass cast that was free to pivot in the horizontal plane about the attachment point. The manipulator was instrumented to measure the displacements of the subject's hand and the forces applied between the subject and the manipulator. Endpoint forces were measured using a six-axis force and moment transducer (JR3 Inc., Woodland, CA; model 30E15A-0560A) with a range of ±334 N. This device has less than 0.1% nonlinearity throughout the measurement range and noise levels less than 0.1 N_{rms}. Endpoint displacement was measured using optical rotary encoders on each joint of the manipulator (DRC, Wilmington, MA; Models 151/EE3–09). These encoders have an effective resolution of 0.0072°, corresponding to an endpoint resolution better than 0.06 mm in the workspace used for these experiments.

Subjects and protocol

Five healthy subjects ranging from 22 to 40 years old and with no history of neurological impairments were used in this study. Subjects gave informed consent to all procedures and were free to withdraw from the study at any time. All measurements were made on the right arm, which happened to be the dominant arm of each subject.

To observe how endpoint stiffness varied as a function of endpoint location, measurements were made at three locations in a horizontal workspace at the vertical level of the glenohumeral joint. All positions were approximately 0.3 m anterior to the acromion. The medial position (M) was in front of the sternum, the central position (C) in front of the acromion, and the lateral position (L) approximately 0.2 m to the right of the acromion. Subjects were secured in the experimental apparatus at the approximate locations described above; the resulting joint angles and endpoint locations were then digitized using an Optotrak system (Northern Digital, Waterloo, Ontario). Table 1 gives the measured joint angles and endpoint locations for each subject.

Prior to each experiment, 12 maximum voluntary contractions (MVCs) were measured for each subject. These corresponded to the maximum endpoint force generated in four directions (parallel to the ±*X*- and ±*Y*-axes shown in Fig. 1) at each of the three endpoint locations. The minimum of these 12 MVCs was used to scale the subjects' voluntary effort in all remaining trials. Table 1 provides the maximum force (30% MVC in the weakest direction) used for each subject.

During each trial, subjects were instructed to exert a constant force against the manipulator in one of the four directions shown in Fig. 1 (±*X* and ±*Y*). For each force direction, the same four absolute force magnitudes were tested: 7.5%, 15%, 22.5%, and 30% MVC (in the weakest direction). In addition, one trial was performed while the subject was at rest, exerting no voluntary endpoint force on the manipulator. Subjects were assisted in this task by a visual display of the endpoint force and the force target.

Figure 2A shows typical endpoint displacements and forces recorded for a single trial. The dashed vertical lines indicate time points when the experimental conditions changed. To obtain baseline values, data from the first 2 s (labeled *a*) in each trial were recorded while the subject was at rest. After 2 s, an auditory cue instructed the subject to generate an endpoint force to match the target force. The subject was then given 4 s (*b*) to reach the force target, after which the manipulator applied a two-dimensional stochastic position perturbation to the subject's hand. This perturbation lasted for 35 s, but only the final 30 s of data (*c*) were used for dynamic stiffness estimation to eliminate any startup transients from the analysis. During the perturbation, endpoint displacements had peak-to-peak amplitudes of approximately 2 cm in each direction. The evoked endpoint force amplitudes varied from trial to trial depending upon arm stiffness. The endpoint displacement frequency content was designed to be within the range of physiologically encountered perturbations (Mann et al. 1989) yet contain enough information for adequate identification of the endpoint dynamics. Figure 2B shows the spectra of the endpoint perturbations used in this study. These perturbations were flat to 3 Hz, above which they decayed at a rate of 40 dB/decade.

Analytical

Nonparametric endpoint stiffness estimation

Endpoint stiffness describes the dynamic relationship between displacements imposed at the hand and the forces resisting those

Table 1 Subject-dependent experimental parameters showing humeral length (L_h) and forearm length (L_f) for each subject, as well as the joint angles and corresponding endpoint locations for each tested arm posture. *Rightmost column* shows the maximum endpoint force tested for each subject. This was 30% of each subject's MVC, as described in the text

Subject	Link lengths (m)		Arm orientation (deg, m)												Maximum tested load (N)
			Medial				Central				Lateral				
	L_h	L_f	θ_s	θ_e	x	y	θ_s	θ_e	x	y	θ_s	θ_e	x	y	
1	0.33	0.32	62.8	102.4	–0.16	0.37	41.7	103.3	–0.02	0.40	14.1	103.8	0.17	0.36	60
2	0.27	0.30	46.8	115.5	–0.10	0.29	21.4	120.6	0.01	0.28	–2.5	102.5	0.21	0.29	24
3	0.29	0.33	48.0	112.8	–0.12	0.33	19.5	117.9	0.03	0.32	3.5	99.2	0.22	0.34	54
4	0.30	0.32	47.1	121.9	–0.11	0.28	23.3	124.6	0.01	0.29	–3.5	111.0	0.20	0.29	45
5	0.34	0.33	57.7	119.8	–0.15	0.30	27.2	120.5	0.02	0.33	–1.6	111.3	0.23	0.30	72

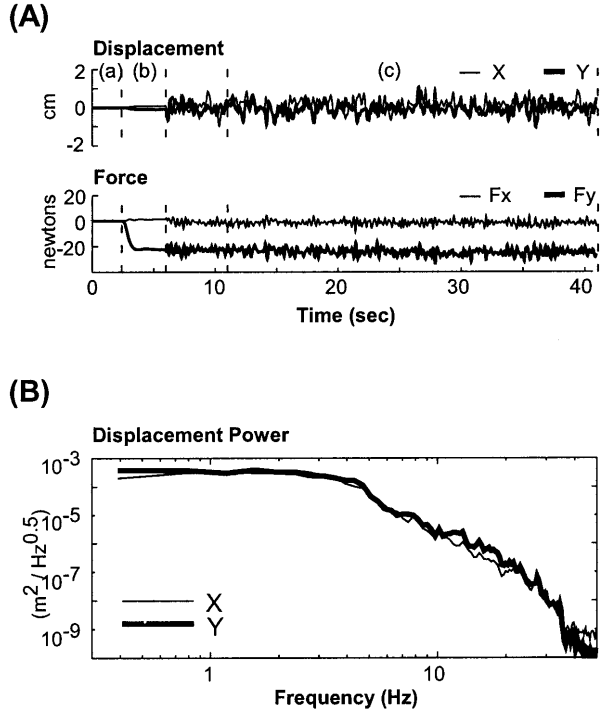

Fig. 2A, B Typical data. **A** shows typical endpoint displacements and forces. Data from the first 2 s (*a*) in each trial were used to record baseline values. After 2 s, an auditory cue instructed the subject to generate an endpoint force to match the target force. The subject was given 4 s (*b*) to reach the force target, after which the manipulator applied a stochastic position perturbation to the subject's hand. The final 30 s of data (*c*) were used for dynamic stiffness estimation. **B** shows the power spectrum of the applied position perturbations

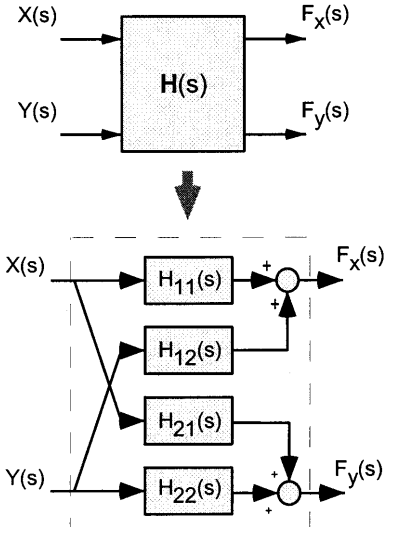

Fig. 3 SISO representation of endpoint stiffness dynamics, illustrating the decomposition of the endpoint stiffness dynamics into a group of SISO systems relating each endpoint displacement to each corresponding force

displacements. The measurements in these experiments were restricted to the horizontal plane, so the goal of the analysis procedures was to estimate the dynamic relationship between endpoint displacements and endpoint forces in the horizontal plane.

Stiffness dynamics were estimated using a robust and efficient nonparametric system identification algorithm described previously (Perreault et al. 1999). The primary assumption of this algorithm is that the endpoint stiffness dynamics can be approximated by a linear system for small perturbations of hand posture. This assumption has previously been validated both experimentally and in simulation (Dolan et al. 1993; Tsuji et al. 1995; Perreault et al. 1999; Stroeve 1999). In general, any linear multiple-input, multiple-output (MIMO) system can be decomposed into the linear subsystems relating each input to each output. Figure 3 illustrates this decomposition for planar endpoint stiffness dynamics. The nonparametric algorithm estimates the optimal (least squares) linear model for each of these single-input, single-output (SISO) subsystems. The dynamics equations describing the relationship between endpoint displacements and endpoint forces can be expressed succinctly in the frequency domain by Eq. 1, where f is frequency, $F_x(f)$ and $F_y(f)$ are the Fourier transforms of the endpoint forces, $X(f)$ and $Y(f)$ are the Fourier transforms of the endpoint displacements, and $H_{ij}(f)$ is the transfer function relating displacements in direction j to forces in direction i.

$$\begin{bmatrix} F_x(f) \\ F_y(f) \end{bmatrix} = \begin{bmatrix} H_{xx}(f) & H_{xy}(f) \\ H_{yx}(f) & H_{yy}(f) \end{bmatrix} \begin{bmatrix} X(f) \\ Y(f) \end{bmatrix} \tag{1}$$

The overall nonparametric fit for each data set was evaluated using the multiple correlation coefficient, R^2, of $f_i(t)$ and $\hat{f}_i(t)$ in Eq. 2. $f_i(t)$ denotes the measured endpoint forces and $\hat{f}_i(t)$ denotes those predicted from the measured endpoint displacements transformed by the estimated nonparametric transfer functions.

$$R^2 \equiv 1 - \frac{\sum_{i\in[x,y]} E\left[\left(f_i(t) - \hat{f}_i(t)\right)^2\right]}{\sum_{i\in[x,y]} E\left[f_i(t)^2\right]} \tag{2}$$

Coherence estimates were used to determine frequency ranges where the linear approximation of the endpoint dynamics fit the data well. Coherence ranges from 0 to 1, with regions of low coherence indicating insufficient input power, significant system nonlinearities, noise, or contributions from unmeasured inputs (Marmarelis and Marmarelis 1978). The *multiple* coherence functions for the dynamic stiffness estimates show the degree to which output forces along each axis of measurement can be linearly predicted using both input displacements. They also indicate the frequencies over which a linear model accurately characterizes the endpoint stiffness dynamics. *Partial* coherence provides an estimate of the linearity of the relationship between single inputs and outputs. These estimates are equivalent to ordinary coherence estimates after the effects of all other inputs have been removed from both the input and output of interest (Bendat and Piersol 1986).

Parameterization of transfer functions

Previous experimental studies have shown that, for small perturbations, each of the SISO systems contributing to the net endpoint stiffness dynamics of the human arm can be approximated by a system having inertial (I), viscous (B) and elastic (K) parameters (Dolan et al. 1993; Tsuji et al. 1995), as shown in Eq. 3. This parametric approximation to the endpoint dynamics was also adequate for the experimental data obtained here. Inertial, viscous and elastic parameters were fit to each of the nonparametric transfer functions using a Nelder-Mead multidimensional optimization algorithm in Matlab (The Mathworks, Natick, MA). During the fitting process, the squared error between the nonparametric and parametric transfer functions was weighted across frequencies by the partial coherence to reduce the influence of poorly estimated portions of the transfer functions.

We assumed that endpoint inertia was invariant across all trials at each arm posture. The most reliable inertial estimates are obtained at rest, where the relative contributions of endpoint viscosity and elasticity are small. Therefore, endpoint inertia, viscosity and elasticity were estimated for the passive trials, but inertia was held constant at this passive estimate when estimating the endpoint viscosity and elasticity during the active trials. The resulting parameterized system had the form given by Eq. 4. I_{end}, B_{end}, and K_{end} correspond to the endpoint inertia, viscosity, and elasticity matrices, respectively.

$$H_{ij}(s) = I_{ij}s^2 + B_{ij}s + K_{ij} \quad \text{where} \quad s = 2\pi f\sqrt{-1} \tag{3}$$

$$[I_{end}]\begin{bmatrix}\ddot{x}\\ \ddot{y}\end{bmatrix} + [B_{end}]\begin{bmatrix}\dot{x}\\ \dot{y}\end{bmatrix} + [K_{end}]\begin{bmatrix}x\\ y\end{bmatrix} = \begin{bmatrix}f_x\\ f_y\end{bmatrix};$$

where

$$[I_{end}] = \begin{bmatrix}I_{xx} & I_{xy}\\ I_{yx} & I_{yy}\end{bmatrix}, \quad [B_{end}] = \begin{bmatrix}B_{xx} & B_{xy}\\ B_{yx} & B_{yy}\end{bmatrix},$$
$$[K_{end}] = \begin{bmatrix}K_{xx} & K_{xy}\\ K_{yx} & K_{yy}\end{bmatrix} \tag{4}$$

The dynamic stiffness of the elbow and shoulder joints and the coupling stiffnesses acting between these joints provide insight to the physiological mechanisms underlying the measured endpoint behavior. These joint-level dynamic stiffness parameters were computed directly from the estimated endpoint parameters using the following transforms:

$$\begin{aligned} K_{jnt} &= J^T \cdot K_{end} \cdot J + \tfrac{\partial J^T}{\partial \Theta} F_{end} \\ B_{jnt} &= J^T \cdot B_{end} \cdot J \\ I_{jnt} &= J^T \cdot I_{end} \cdot J \\ J &= \begin{bmatrix} -l_h\sin(\theta_s) - l_f\sin(\theta_s+\theta_e) & -l_f\sin(\theta_s+\theta_e) \\ l_h\cos(\theta_s) + l_f\cos(\theta_s+\theta_e) & l_f\cos(\theta_s+\theta_e)\end{bmatrix} \end{aligned} \tag{5}$$

J is the Jacobian relating differential changes in joint rotation to differential changes in endpoint displacement, l_h and l_f are the lengths of the humerus and forearm, θ_s and θ_e are the shoulder and elbow angles, and F_{end} is the steady state endpoint force vector. The additional term in the elastic stiffness transformation is due to the geometry of the arm and the constant forces exerted voluntarily by the subject and acting at the endpoint (McIntyre et al. 1996). The Jacobian can also be used to obtain shoulder and elbow joint torques (TQ) from the measured endpoint forces as shown in Eq. 6.

$$\begin{bmatrix}TQ_s\\ TQ_e\end{bmatrix} = J^T\begin{bmatrix}f_x\\ f_y\end{bmatrix} \tag{6}$$

Parameter error estimation

The estimation errors associated with the nonparametric system identification algorithm and the subsequent parameter fits were evaluated using Monte Carlo simulations. For each trial, the estimated nonparametric transfer functions were assumed to represent the "true" endpoint stiffness dynamics. One hundred simulated data sets were generated by convolving these same four transfer functions with different endpoint displacements (each independent but with the same statistical properties as the experimental displacements), creating simulated endpoint forces. Randomly generated "measurement" noise, matched to the power spectra and standard deviation of the experimental measurement noise, was also added to each of the simulated force responses. The system identification and parameter fitting algorithms described above were applied to each of the simulated data sets. Confidence intervals on the parameter estimates for each trial were then estimated using the standard deviation of these parameters across all 100 simulated trials.

Graphical representation of parameter fits

The inertial, viscous and elastic properties of the arm are directionally dependent, meaning that the resistance they provide to external perturbations of hand posture depends upon the orientation of the perturbation. This dependence on direction can be represented graphically by transforming the inertial, viscous and elastic matrices into ellipses, as was first demonstrated by Mussa-Ivaldi (1985). Equation 7 shows how this mapping is achieved for the endpoint elasticity matrix, K_{end}. The variables $F^K_y(t)$ and $F^K_x(t)$ represent the elastic components of the force response for unit displacements of the hand in endpoint position along all directions in the plane; these unit displacements are generated using the *sin* and *cos* functions in Eq. 7. The ellipse representing the directional properties of K_{end} is generated by plotting $F^K_y(t)$ against $F^K_x(t)$. A similar procedure is used to generate the viscosity and inertial ellipses.

$$\begin{bmatrix}F^K_x(t)\\ F^K_y(t)\end{bmatrix} = K_{end}\cdot\begin{bmatrix}\cos(t)\\ \sin(t)\end{bmatrix}; \quad \text{where} \quad 0 < t < 2\pi \tag{7}$$

The major axis of the K_{end} ellipse denotes the direction along which the endpoint of the arm is most resistant to displacements of posture, while the minor axis indicates the direction of least resistance to these disturbances. The elastic stiffness ellipse can thus be characterized by the orientation of the major axis, ϕ, the "shape" s (ratio of the minor to major axes), and the area, A. The equations needed to calculate each of these parameters were presented by Gomi and Osu (1998), and are repeated below for completeness. Note that they do not require K_{end} to be symmetric and that $\lambda(.)$ represents the eigenvalue operator.

$$\phi = \tan^{-1}\left(\frac{U_{\max\_y}}{U_{\max\_x}}\right) \tag{8}$$

where U_{max_x} and U_{max_y} are obtained via singular value decomposition of the K_{end} matrix, as shown in Eq. 9. S is a diagonal matrix containing the singular values of K_{end}, and U and V contain the

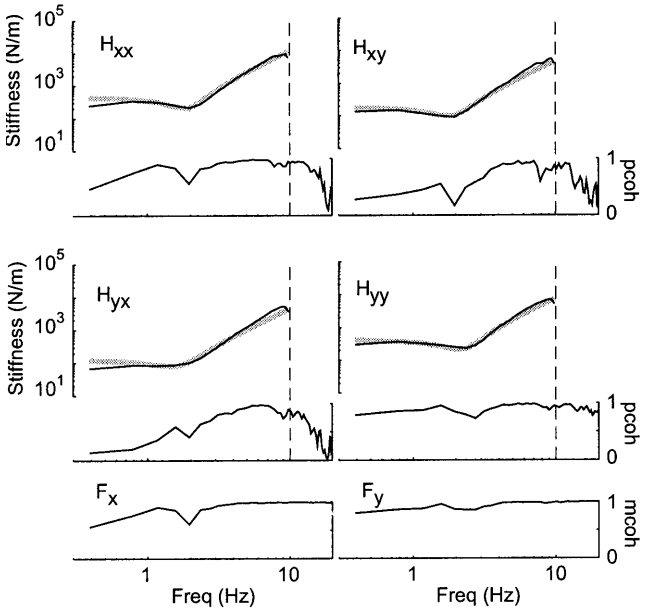

Fig. 4 Nonparametric transfer functions and coherence. *The thin black lines* illustrate typical estimated nonparametric stiffness transfer functions and the corresponding partial coherences relating endpoint displacements and endpoint forces. *The bottom two figures* are the multiple coherence functions for each output. *Thick, gray lines* indicate the second-order parametric approximations to these transfer functions. *Vertical dashed lines* are drawn at 10 Hz, the highest frequency used in the parametric fit

orthogonal eigenvectors of $K_{end} \cdot K_{end}{}^T$ and $K_{end}{}^T \cdot K_{end}$, respectively (Strang 1998).

$$K_{end} = U \cdot S \cdot V^T, \quad \text{and} \quad U = \begin{bmatrix} U_{\max\_x} & U_{\min\_x} \\ U_{\max\_y} & U_{\min\_y} \end{bmatrix} \tag{9}$$

$$shape = \frac{\alpha_{\min}}{\alpha_{\max}}, \quad \text{where} \quad \alpha_{\min} = \sqrt{\lambda_{\min}\left(K_{end}^T \cdot K_{end}\right)} \quad \text{and} \quad \alpha_{\max} = \sqrt{\lambda_{\max}\left(K_{end}^T \cdot K_{end}\right)} \tag{10}$$

$$Area = \pi \alpha_{\min} \alpha_{\max} \tag{11}$$

Results

Identification and parameter fitting

Figure 4 illustrates the magnitude portion of typical endpoint stiffness transfer functions. The linear, nonparametric descriptions of endpoint stiffness used in this study were found to provide good descriptions of the experimental data, with an average R^2 across all trials and all subjects of 94.6±2.6%. Figure 4 also shows the second-order approximation to these functions (gray lines), and the corresponding partial (pcoh) and multiple coherences (mcoh). The multiple coherence functions remained high between 1 and 30 Hz, indicating that, over this frequency range, the endpoint force responses to the applied position disturbances were well characterized by the nonparametric linear models. The partial coherences between each input and each output are shown below the corresponding transfer functions. For all subjects, partial coherence began to decline below approximately 1 Hz and above approximately 10 Hz. The decrease above 10 Hz arises from the fact that there was little *input* power at higher frequencies (see Fig. 2B). For this reason, parametric fits to the nonparametric transfer functions were performed only below 10 Hz, as indicated by the dashed lines in Fig. 4. The decrease below 1 Hz is likely due to low frequency tracking errors as subjects attempted to maintain the target force. Occasionally, decreases in partial coherence near the transfer function resonant frequency were also observed (see H_{xx}), due to decreased *output* power near these frequencies (Hunter and Kearney 1982). Because our estimation algorithm was insensitive to output (force) noise (Perreault et al. 1999), the low frequency coherence decreases do not bias our transfer function estimates.

The near perfect overlap of the nonparametric transfer functions and the second-order fits indicates that the endpoint dynamics estimated for this trial were well approximated by a system with inertial, viscous and elastic components. The errors associated with this parameterization were estimated using the Monte Carlo simulations described above. The average parameter standard deviations for the inertial, viscous and elastic estimates were 0.033 N·s^2/m, 1.12 N·s/m, and 24.0 N/m, respectively, across all subjects and all endpoint forces. Note that inertia, viscosity and elasticity parameter magnitudes had maximum values of approximately 3 N·s^2/m, 40 N·s/m, and 1500 N/m, respectively, across all subjects and forces. For all parameters, the standard deviation of the estimate did not increase with increases in the mean value of the estimate, indicating that the relative error was smallest for the larger parameter values.

Changes in endpoint elasticity

For all subjects, the elastic properties of the arm depended on both the endpoint location and the level of voluntary force generation. Figure 5 illustrates typical elasticity ellipses for all trials of a single subject at each endpoint location. These ellipses are positioned at a location proportional to the force magnitude and in the direction that the subject was exerting this force against the manipulator. The thin straight lines indicate arm orientation, with the hand located at the center of each group of ellipses. The endpoint stiffness ellipses are seen to increase in magnitude with increasing endpoint force and to have shapes and orientations that are dependent upon force direction.

All components of the endpoint stiffness matrix scaled linearly with endpoint force, and for all conditions the cross-terms, K_{xy} and K_{yx}, were nearly equal, resulting in predominantly symmetric endpoint stiffness matrices. Figure 6 shows typical data for one subject at the central endpoint position. In this figure, the circles correspond to the elastic stiffness estimated during each trial and the error bars indicate the standard deviation of these

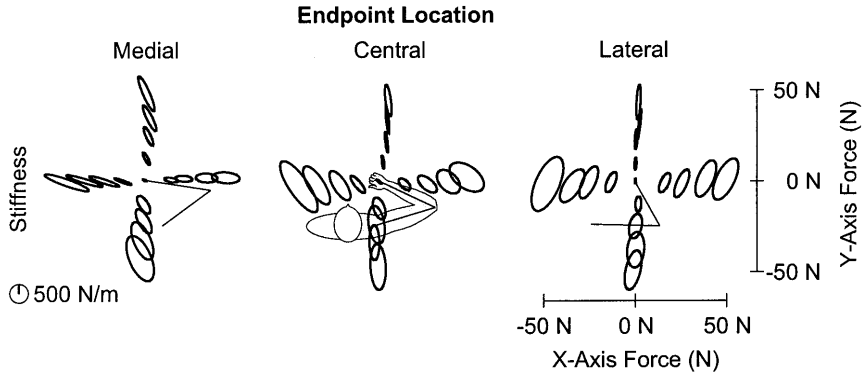

Fig. 5 Typical variations in elastic endpoint stiffness, illustrating results from all trials of a single subject (no. 4) at each endpoint location. Ellipses are positioned at a location proportional to the force magnitude and in the direction that the subject was exerting this force against the manipulator. *The thin straight lines* indicate arm orientation, with the hand located at the center of each group of ellipses

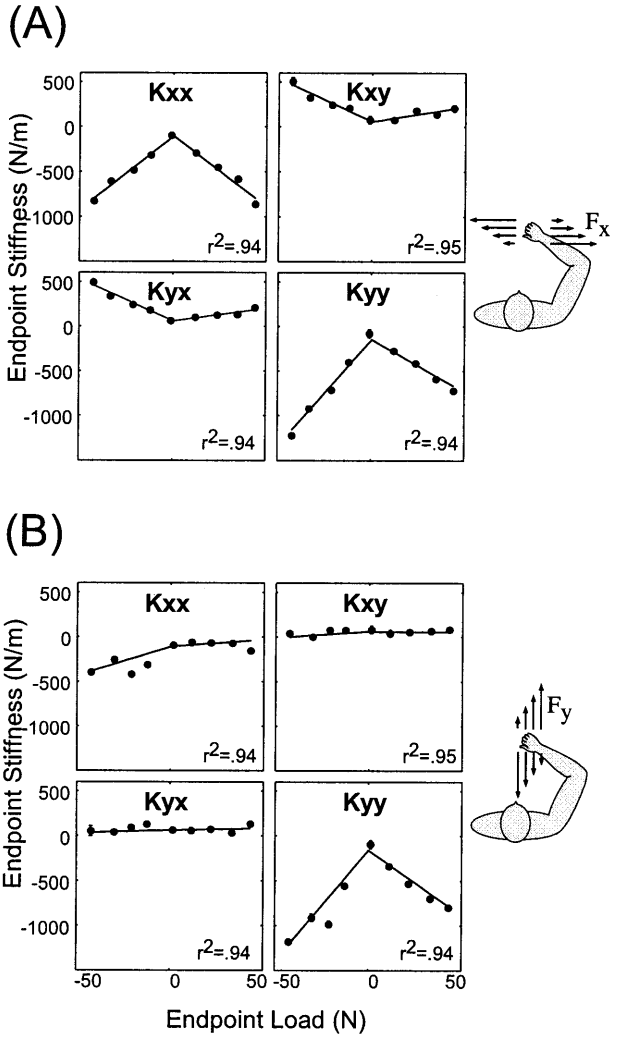

Fig. 6A, B Variations in endpoint stiffness parameters with endpoint force. Typical data for a single subject (no. 4) illustrating changes in endpoint stiffness with endpoint force. **A** shows how each component of the elastic endpoint stiffness matrix scaled with changes in endpoint force along the *X*-axis. **B** shows how these parameters varied with changes in force along the *Y*-axis. *Error bars* indicate ±1 SD

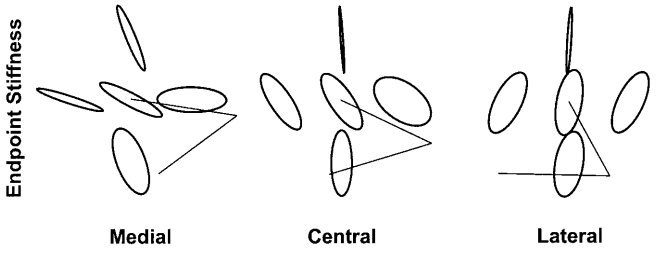

Fig. 7 Variations in endpoint stiffness shape and orientation with force direction. Typical changes in endpoint stiffness shape and orientation for subject no. 4 at 30% MVC. The plotted stiffnesses were generated using Eq. 12, which was fit to all data collected at each endpoint location. These ellipses are normalized by their maximal eigenvalue, and therefore only indicate orientation and shape, not size. *The central ellipse* in each figure corresponds to the elastic endpoint stiffness when the subject is at rest; *the other four ellipses* represent the elastic stiffness when this subject was exerting force in the direction of the plotted ellipse

estimates. In most cases, the standard deviations are small enough to be obscured by the circles representing the data points. Figure 6A shows how each component of the elastic stiffness matrix scaled with changes in endpoint force along the *X*-axis and Fig. 6B shows how these parameters varied with changes in endpoint force along the *Y*-axis. Because each component of the endpoint elasticity scaled linearly with endpoint force, the stiffness-force relationship could be characterized by Eq. 12. In this equation, F_x^+ denotes the force along the positive *X*-axis, F_x^- is the force along the negative *X*-axis, and F_y^+ and F_y^- are the analogous forces along the *Y*-axis. For each subject, this equation was fit to each component of the endpoint elasticity matrix at each endpoint location using linear regression. The fitted models accounted for 94±4% of the endpoint elasticity variance across all subjects, endpoint forces, and endpoint locations. The solid lines in Fig. 6 illustrate a typical fit.

$$K_{ij}^{end} = \alpha_0 + \alpha_{Fx}^{+}\left|F_x^{+}\right| + \alpha_{Fy}^{+}\left|F_y^{+}\right| + \alpha_{Fx}^{-}\left|F_x^{-}\right| + \alpha_{Fy}^{-}\left|F_y^{-}\right| \quad (12)$$

Endpoint force magnitude and direction significantly modified the shape and orientation of the endpoint elasticity ellipses. Figure 7 shows typical changes in end-

Table 2 Effects of endpoint force on shape and orientation, showing the minimum and maximum ellipse orientations and shapes for all subjects at each endpoint location over the range of tested forces

Subject	Endpoint location	Orientation (deg)			Shape		
		Min	Max	Range	Min	Max	Range
1	M	105.4	147.9	42.5	0.07	0.55	0.48
	C	92.9	124.5	31.6	0.09	0.56	0.47
	L	65.5	85.7	20.2	0.15	0.46	0.31
2	M	109.8	159.8	50.0	0.14	0.44	0.30
	C	95.3	122.8	27.5	0.12	0.49	0.37
	L	62.0	87.5	25.5	0.05	0.33	0.28
3	M	105.1	166.2	61.1	0.05	0.56	0.51
	C	80.2	123.6	43.4	0.13	0.73	0.60
	L	71.0	86.9	15.9	0.04	0.47	0.43
4	M	111.5	179.0	67.5	0.11	0.41	0.30
	C	90.2	144.8	54.6	0.04	0.57	0.53
	L	63.1	86.6	23.5	0.06	0.43	0.37
5	M	113.6	172.6	59.0	0.10	0.54	0.44
	C	92.4	139.4	47.0	0.13	0.71	0.58
	L	67.3	84.6	17.3	0.12	0.45	0.33

point stiffness shape and orientation for one subject at the maximum forces used in this study (30% MVC). The plotted ellipses were generated using Eq. 12, which was fit to all data collected at a given endpoint location. These ellipses are normalized by their maximal eigenvalue, and therefore only indicate orientation and shape, not size. The central ellipse in each figure corresponds to the endpoint elasticity when the subject is at rest. Each of the other four ellipses represents the elasticity when the subject was exerting force in the direction of the plotted ellipse at 30% MVC. It is clear from Fig. 7 that the changes in orientation and shape with force were largest in this subject for the more medially located endpoint positions. These results are summarized for all subjects in Table 2, which shows the minimum and maximum ellipse orientations and shapes at each endpoint location for the range of tested experimental forces. The endpoint force effects (magnitude and direction) on endpoint stiffness orientation were greatest for the medial posture in all subjects, with an average maximal change in orientation of 56°. Maximal variations in shape occurred at the central posture for four/five subjects and at the medial posture for the remaining subject, with an average maximal change in ellipse shape of 0.51. Voluntarily generated endpoint forces directed away from the shoulder and elbow joints decreased shape, resulting in a thinner endpoint stiffness ellipse while those directed toward the shoulder and elbow joints tended to increase shape, resulting in a broader stiffness.

Changes in joint elasticity

Postural independence

As illustrated in Eq. 5, endpoint stiffness is directly related to the joint stiffnesses of the shoulder and elbow. It was found that joint stiffnesses computed from endpoint stiffness estimates in this way could be well predicted

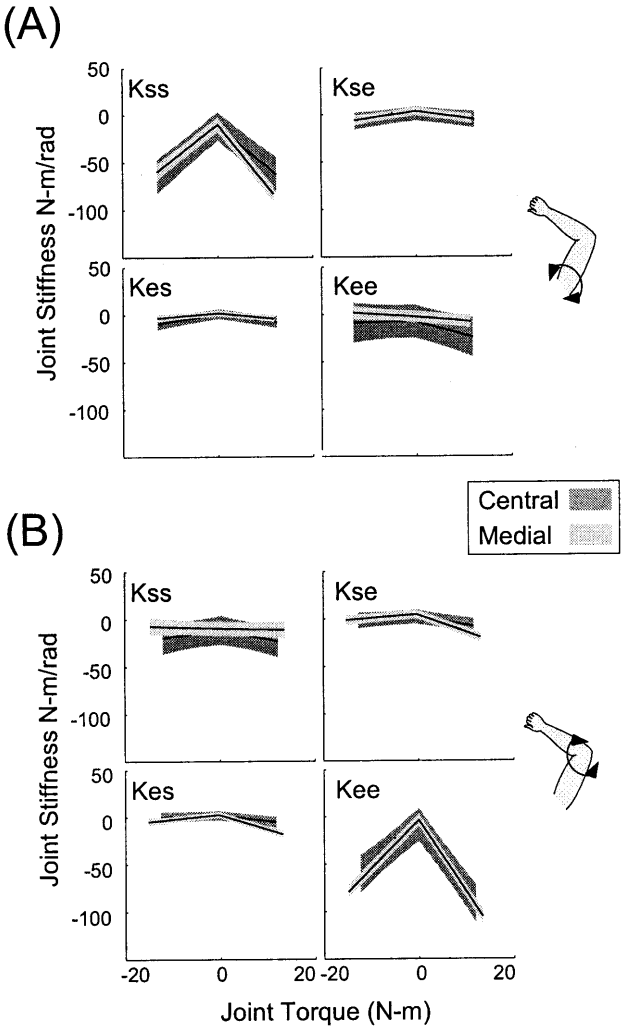

Fig. 8A, B Variations in joint stiffness parameters with joint torque. Estimated joint torque-stiffness relationships for subject no. 4 at two different endpoint locations, the medial and central postures. *The solid lines* indicate the model predictions, and *the gray bars* indicate the ±95% confidence intervals for these predictions. **A** shows the effects of changes in shoulder joint torque on the joint-level elastic stiffness parameters, and **B** shows the effects of changes in elbow joint torque

from joint torques using Eq. 13, which is simply the joint coordinate version of Eq. 12. The average r^2 for fits to the data at each endpoint location was 0.90±0.09 across all subjects, indicating that the joint torque-joint stiffness relationship was approximately linear. This finding is in agreement with the results of numerous studies (Agarwal and Gottlieb 1977; Cannon and Zahalak 1982; Hunter and Kearney 1982; Weiss et al. 1988; Kirsch and Rymer 1992; Gomi and Osu 1998).

$$K_{ij}^{Joint} = \alpha_0 + \alpha_{TQs}^{+}\left|TQ_s^{+}\right| + \alpha_{TQe}^{+}\left|TQ_e^{+}\right| + \alpha_{TQs}^{-}\left|TQ_s^{-}\right| + \alpha_{TQe}^{-}\left|TQ_e^{-}\right| \quad (13)$$

Figure 8 shows the estimated joint torque-stiffness relationships for one subject at two different endpoint loca-

Table 3 Modulation of joint stiffness with joint torque. These regression parameters characterize changes in joint stiffness with changes in joint torque. Parameters were obtained by combining the experimental data at all endpoint locations and fitting to Eq. 13

Subject	Joint stiffness	α_0	α^+_{TQs}	α^+_{TQe}	α^-_{TQs}	α^-_{TQe}	r^2
1	*Kss*	–23.26±8.14*	–3.01±0.79*	–0.94±1.09	–2.97±0.82*	–0.30±1.08	0.72
2	*Kss*	–7.85±2.22*	–3.98±0.73*	–1.09±0.81*	–4.41±0.73*	–0.55±0.75	0.86
3	*Kss*	–15.03±4.94*	–3.86±0.67*	–1.01±0.74*	–3.69±0.67*	–0.64±0.72	0.87
4	*Kss*	–11.06±3.89*	–4.72±0.65*	–0.29±0.62	–4.26±0.62*	–0.05±0.59	0.88
5	*Kss*	–17.45±7.46*	–3.89±0.85*	–1.32±0.86*	–4.35±0.81*	–1.04±0.68	0.83
	Mean	–14.93	–3.89	–0.93	–3.94	–0.52	
1	*Kse*	1.71±3.25	–0.37±0.32*	–2.25±0.43*	–0.56±0.33*	–0.77±0.43*	0.79
2	*Kse*	0.31±1.09	0.04±0.36	–2.35±0.40*	–0.65±0.36*	–0.81±0.37*	0.79
3	*Kse*	0.23±2.34	–0.05±0.32	–2.33±0.35*	–0.96±0.32*	–0.95±0.34*	0.86
4	*Kse*	2.03±2.38	–0.75±0.40*	–1.64±0.38*	–0.72±0.38*	–0.59±0.36*	0.74
5	*Kse*	–0.54±4.03	–0.09±0.46	–1.65±0.46*	–0.37±0.44	–0.31±0.36*	0.61
	Mean	0.75	–0.24	–2.04	–0.65	–0.69	
1	*Kes*	1.88±3.65	–0.63±0.36*	–1.77±0.49*	–0.49±0.37*	–0.86±0.48*	0.71
2	*Kes*	1.38±1.00*	–0.93±0.33*	–1.86±0.36*	–0.49±0.33*	–1.04±0.34*	0.84
3	*Kes*	0.32±2.06	–0.23±0.28	–2.30±0.31*	–0.99±0.28*	–0.83±0.30*	0.89
4	*Kes*	1.72±2.01	–0.72±0.33*	–1.32±0.32*	–0.62±0.32*	–0.60±0.30*	0.74
5	*Kes*	–1.67±4.17	0.38±0.48	–2.09±0.48*	–0.36±0.45	–0.18±0.38	0.66
	Mean	0.73	–0.43	–1.87	–0.59	–0.70	
1	*Kee*	–11.60±4.98*	–0.42±0.49	–5.68±0.67*	–0.08±0.50	–4.97±0.66*	0.91
2	*Kee*	–5.55±1.88*	0.35±0.61	–8.16±0.69*	0.40±0.62	–5.73±0.63*	0.95
3	*Kee*	–11.93±4.70*	1.50±0.64*	–6.72±0.70*	0.53±0.64	–4.83±0.68*	0.91
4	*Kee*	–8.02±3.24*	–0.45±0.54	–7.27±0.52*	–0.05±0.52	–4.65±0.49*	0.96
5	*Kee*	–23.27±8.65*	–0.42±0.99	–6.72±0.99*	–0.60±0.94	–4.09±0.78*	0.86
	Mean	–12.07	0.11	–6.91	0.04	–4.85	

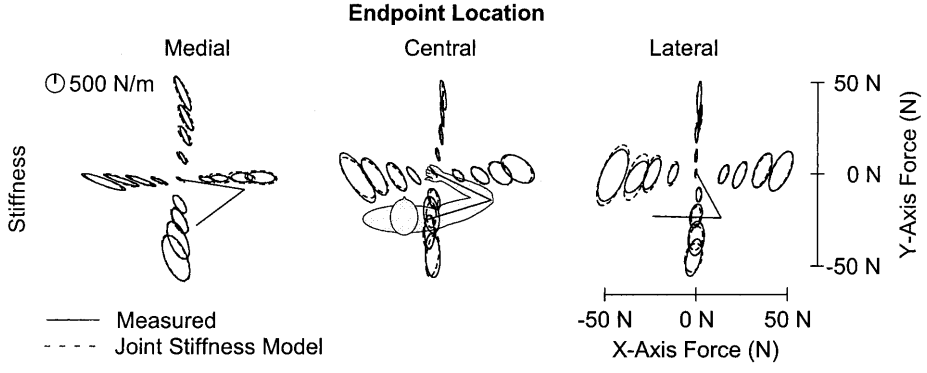

Fig. 9 Endpoint stiffness predictions with posture-independent joint stiffness model, comparing actual endpoint stiffness measurements (*solid*) with predictions made by the posture-independent joint torque-stiffness model (*dashed*)

tions, the medial and central postures. The solid lines indicate the model predictions, and the gray bars indicate the ±95% confidence intervals for these predictions. Figure 8A shows the effects of changes in shoulder joint torque on the joint-level elastic stiffness parameters, and Fig. 8B shows the effects of changes in elbow joint torque on these same parameters. At both endpoint locations, the modulation of the single-joint stiffnesses, *Kss* and *Kee*, with changes in torque about the relevant joint were much greater than those of the cross-joint terms, *Kes* and *Kse*. Although there were some posture-dependent variations in the joint torque-joint stiffness relationships, these effects were very modest across the arm postures studied.

Because the posture-dependent variations in the joint torque-stiffness relationships were small, the data from all locations were used to estimate the average torque-stiffness relationship for a given subject over all studied postures by fitting Eq. 13 to all data for that subject. Table 3 gives the estimated parameter values needed to predict joint stiffness from joint torque for each subject. In this table, α_0 represents the stiffness of each term for rest conditions, and the remaining terms indicate how stiffness was modulated by torque changes in the specified direction. The 95% confidence intervals are provided next to each parameter; all parameters that were significantly different from zero ($P<0.05$) are marked with an asterisk. The average r^2 for all parameter fits across all subjects was 82%, indicating that the torque-stiffness relationships were predominantly independent of posture. The elbow torque-stiffness relationship was most invariant across all postures, with an average r^2 of 0.92 for all subjects. The accuracy of the fits for the shoulder and cross-joint stiffnesses were similar to each other and had values of 0.83 and 0.76 respectively. Thus, the simple model of the joint torque-joint elasticity relationship given by Eq. 13 accurately summarized the experimental endpoint stiffness data at the three postures investigated in this study. This conclusion is emphasized by Fig. 9, which shows the ability of an invariant joint torque-joint

stiffness characteristic to predict the endpoint stiffness ellipses for all arm postures and endpoint forces for a typical subject. The solid ellipses show the measured stiffnesses and the dashed ellipses show the elastic endpoint stiffnesses predicted from the joint torques, using Eqs. 5 and 13. The differences between the estimated elastic stiffnesses and those predicted from the posture-independent joint stiffness model were small for all subjects. The measured and predicted ellipses had mean orientation differences of 0.13±7.32°, mean shape differences of 0.00±0.07, and mean area differences of –9.6±48%. Data from the low force trials had larger area errors than other trials. When the smallest 10% of the ellipses were removed from the analysis, the mean area difference was reduced to –1.5±39%. This is likely due to the near constant estimation errors (see Sect. 3.1), which have a larger percentage influence on predictions of smaller endpoint stiffness areas than larger stiffness areas. The geometric mean of these smallest ellipses (2.6×10^4 N^2/m^2) was approximately one order of magnitude less than the geometric mean of all stiffness ellipses (4.2×10^5 N^2/m^2) and two orders of magnitude less than the largest 10% (2.9×10^6 N^2/m^2).

Role of single-joint muscles

The magnitudes of the parameters in Table 3 indicate the degree to which the joint stiffnesses were affected by changes in shoulder and elbow joint torques. These results show that single-joint stiffnesses were more dependent on changes in joint torques than were cross-joint stiffnesses. In addition, the stiffness at a particular joint was most affected by the torques at that joint, while cross joint stiffnesses were affected by both shoulder and elbow torques. Elbow flexion torques (positive) had a greater effect on cross-joint stiffness than did shoulder flexion torques, but extension torques about both of these joints had similar levels of significance and modulation with respect to the cross-joint stiffnesses. These results are in contrast to those of Gomi and Osu (1998), who found that the cross-joint stiffness parameters were only affected by changes in elbow joint torques. Our results indicate that shoulder torques, especially shoulder extension torques, also contribute to the cross-joint stiffnesses.

Multijoint muscles contributed less to the total arm stiffness than single-joint muscles during these force regulation tasks. The stiffness of a single joint (e.g., *Kss* or *Kee*) is due to the passive stiffness of the joint, the stiffness from the muscles acting about that joint, and the stiffness from multijoint muscles. In contrast, the estimated cross-joint stiffnesses are due only to muscles spanning both joints (see Hogan 1985). Using this additive relationship at individual joints and the mean results presented in Table 3, the relative contributions of active single-joint and multijoint muscles to the estimated single-joint stiffness during voluntary force generation were calculated. The biceps is the multijoint muscle involved in elbow and shoulder flexion and the triceps is the multijoint muscle involved in the extension of these same joints. The maximum multijoint contribution to single joint stiffness was the 28% contribution of the biceps muscle to elbow joint stiffness during elbow flexion. This same muscle contributed only 8% to the estimated shoulder joint stiffness during shoulder flexion. The triceps contributed nearly equally to the elbow and shoulder stiffnesses, accounting for 14% of the elbow stiffness during elbow extension and 16% of the shoulder stiffness during shoulder extension. These results indicate that, in all cases, the active contributions of multijoint muscles to single joint stiffnesses were small relative to those of single joint muscles.

Discussion

This study examined how elastic endpoint stiffness is modulated as voluntary forces are exerted against a rigid environment. Elastic endpoint stiffness describes the relationship between external displacements applied at the hand and the position-dependent forces evoked in response. Thus, it characterizes the elastic properties of the mechanical interface the arm presents to the environment and is thought to be closely related to postural arm stability (Feldman 1966; Bizzi and Abend 1983; Hogan 1985; Colgate and Hogan 1988; Lacquaniti et al. 1993; Gomi and Osu 1998). Understanding how this interface is modulated by the central nervous system may provide insight into how humans consistently make stable interactions with their environment, and maintain stable arm postures in the face of unexpected disturbances. This study focused on the modulation of endpoint stiffness during force regulation tasks. We found that the elastic components of multijoint stiffness scaled linearly with increasing endpoint forces, and that the shape and orientation of this stiffness depended upon force orientation. The observed changes in endpoint stiffness resulted from joint torque-joint stiffness relationships that were predominantly posture independent, thereby allowing endpoint stiffness characteristics to be predicted from arm posture and endpoint voluntary forces. These results may indicate a simplifying strategy that the nervous system uses to control arm mechanics during force regulation tasks.

Methodology

Endpoint stiffness dynamics were estimated by applying small, stochastic position perturbations to the hand, measuring the evoked forces, and using a nonparametric system identification algorithm to estimate the relationship between the two. The large information content in the stochastic perturbation allowed for a rapid characterization of the endpoint mechanics. Similar methods have been applied by numerous laboratories to estimate single-joint mechanics (Agarwal and Gottlieb 1977; Hunter and

Kearney 1982; Lacquaniti et al. 1982; Weiss et al. 1988; Kirsch and Rymer 1992), but have not previously been used to study multijoint systems. Previous studies of multijoint arm stiffness have relied on step or pulse inputs (Mussa-Ivaldi et al. 1985; Dolan et al. 1993; Tsuji et al. 1995; Gomi and Osu 1998). The results of our study are similar to those obtained using different perturbations where the experimental conditions overlapped.

The mechanical response to stretch consists of both intrinsic and reflex mechanisms. Our techniques made no attempt to separate the relative contributions of these mechanisms. Single-joint studies have shown that reflex contributions are greatest at moderate frequencies, typically less than 10 Hz (Bennett 1994; Kearney et al. 1997). Our perturbations had sufficient power to estimate the *net* endpoint dynamics within this range (Figs. 2, 4), and hence our results may be influenced by both intrinsic and reflex mechanisms. Separating these contributions to multijoint stiffness requires an extension of the techniques developed for single joints (Kearney et al. 1997; Zhang and Rymer 1997).

Variations in elastic endpoint stiffness with force

Each component of elastic endpoint stiffness scaled linearly with force magnitude. However, changes in endpoint force direction produced changes in endpoint stiffness shape and orientation, indicating that the mechanical interface presented to the environment depends upon the magnitude and direction of voluntarily generated endpoint forces. These results agree with those of Gomi and Osu (1998), who observed similar variations using smaller endpoint forces. We also found that voluntarily generated endpoint forces directed away from the elbow and shoulder joints decreased shape, creating a narrower, less stable ellipse, in agreement with the stability analysis of McIntyre et al. (1996).

Contrary to our results, other studies have concluded that, at a given posture, stiffness orientation and shape are invariant with respect to the level of voluntary effort (Mussa-Ivaldi et al. 1985; McIntyre et al. 1996). The conditions of these previous experiments differed significantly from our own. Both used long (>1.0 s) step changes in endpoint position to estimate stiffness, with the significant possibility of voluntary interventions. Mussa-Ivaldi measured endpoint stiffness immediately *after* an oscillating force was applied to the hand, not while a force was present. McIntyre used large, static forces, but only for restricted force directions at a single arm posture. Both studies also required subjects to grasp a handle on the manipulator, which may have led to higher levels of cocontraction than required by our protocol (see Tsuji et al. 1995). We therefore believe that the variations in endpoint stiffness orientation and shape observed here occur naturally as the arm exerts forces against the environment and that these variations reflect normal geometric and neural constraints.

Postural independence of joint stiffness

For all voluntary endpoint forces, endpoint elasticity orientation depended strongly on hand location. The orientation rotated clockwise as the hand moved from medial to lateral positions. Similar results were first reported by Mussa-Ivaldi et al. (1985) and have been replicated many times (Dolan et al. 1993; Tsuji et al. 1995; Gomi and Osu 1998). We sought to determine if this postural dependence was simply due to arm geometry, or if it represents a more complicated control strategy. Flash and Mussa-Ivaldi (1990) previously posed this same question, but only for cases where the subject was at rest. Our results indicate that, during force regulation tasks, the posture dependent variations in endpoint stiffness are due primarily to the corresponding changes in arm geometry and not to an underlying neural control strategy. This was demonstrated using a constant joint torque-joint stiffness relationship to accurately predict endpoint stiffness variations with changes in endpoint force throughout the studied workspace. Gomi and Osu (1998) computed joint torque-stiffness relationships at several arm configurations but did not examine the invariance of this characteristic with respect to joint posture. However, the high correlations they reported for the torque-stiffness relationships across all postures appear to agree with our results. Our conclusions contradict the conclusions of Flash and Mussa-Ivaldi (1990), who observed posture-dependent changes in joint stiffness. However, their study was performed with no voluntary endpoint forces. It thus appears that during active force regulation tasks, the joint torque-stiffness characteristics are independent of arm posture.

Role of single-joint and double-joint muscles during force regulation

For the force regulation tasks used in this study, the single-joint stiffnesses were significantly larger than the cross-joint stiffnesses and were strongly modulated by torques about the same joint. Joint torque increases resulted in corresponding single-joint stiffness increases, as shown in many single-joint studies (Agarwal and Gottlieb 1977; Cannon and Zahalak 1982; Hunter and Kearney 1982; Weiss et al. 1988; Kirsch and Rymer 1992), and the one published multijoint study (Gomi and Osu 1998) that examined joint stiffness torque relationships. The single-joint torque-stiffness slopes (α^{+}_{TQe}) reported here [approximately 6.9 (N-m/rad)/(N-m)] are similar to those reported by Gomi and Osu (1998), but are higher than those [3.6 (N-m/rad)/(N-m)] found in previous single-joint studies of elbow joint stiffness (Kirsch and Rymer 1992; Zhang and Rymer 1997). This difference may represent increased cocontraction to generate the precise endpoint forces used in this study as opposed to the single-joint torques used in the previous works.

Except for elbow flexion, the modulation of two-joint stiffnesses with changes in joint torques was minimal

compared to that of the single-joint stiffnesses, indicating that multijoint muscles contributed relatively little to the net arm stiffness during force regulation tasks. This decreased dependence on two-joint muscles during force regulation tasks explains the observed postural independence of stiffness at the joint level and may imply a simplifying neural control strategy for regulating endpoint forces and arm mechanics during isometric endpoint force generating tasks. Contributions of an individual muscle to joint stiffness depend on muscle stiffness, which increases with muscle activation (Hoffer and Andreassen 1981; Kirsch et al. 1994), and on moment arm length. Both of these factors may contribute to the observed results. While joint torque scales with moment arm length, stiffness scales with the square of this length. This relationship explains why the biceps, with an elbow moment arm approximately twice that of its shoulder moment arm (van der Helm et al. 1992), has a much larger effect on elbow stiffness than shoulder stiffness. Such moment arm differences between single-joint and cross-joint muscles may also contribute to the relatively small cross-joint stiffnesses observed in this study. For example, the moment arms of the brachioradialis and pectoralis muscles (both single-joint muscles) are significantly larger than their cross-joint counterparts (van der Helm et al. 1992). Relatively low activations of the two-joint muscles during the studied tasks would also account for their decreased role in regulating net arm stiffness. Previous studies at single joints (Tax et al. 1990; van Groeningen and Erkelens 1994; van Bolhuis and Gielen 1997) have shown that cross-joint muscles are less active during force regulation than during position regulation. Similar behavior during multijoint tasks would help to explain the findings of this study, but such detailed estimates of muscle activation during multijoint tasks are not currently available. Therefore, additional study is required to separate the relative importance of moment arms and muscle activation to the stiffness relationships measured in these experiments.

Task dependence of endpoint stiffness

The tasks examined in this study were limited to subjects generating controlled forces against a quasi-isometric manipulator, so we cannot currently extend our conclusions to movement or other postural conditions. For example, it is likely that a more complex control strategy is necessary for regulating endpoint position than for regulating endpoint force. Single-joint studies have shown that cocontraction increases when subjects switch from force regulation to position regulation, thereby resulting in a higher elastic stiffness (Akazawa et al. 1983; De Serres and Milner 1991). If the increased stability results from cocontraction of two-joint muscles, which are thought to have a unique role in stabilizing arm posture (McIntyre et al. 1996), the postural independence of the joint torque-stiffness relationship found in this study might not hold for position regulation tasks. The control of movement may also differ. The two-joint muscles crossing the shoulder and elbow are more active during movement than during isometric force generation tasks (Tax et al. 1990; van Groeningen and Erkelens 1994; van Bolhuis and Gielen 1997), and the ratio of cross-joint stiffness to elbow stiffness is larger during movement than during posture maintenance (Gomi and Kawato 1997), pointing to different control strategies for movement and for posture maintenance. Our results do suggest that stiffness properties during movements made against even modest loads may be significantly different from the unconstrained arm movements that have dominated studies in the past. Further study of task dependent multijoint stiffness regulation are required to determine the relative roles of load dependent stiffness changes and neurally mediated interjoint coordination.

Acknowledgement This work was supported by the Department of Veteran Affairs Rehabilitation Research and Development Service, the National Institute of Health, and the Cleveland FES Institute. The authors would also like to thank Dr. C.J. Heckman for his insightful comments on this manuscript.

References

Acosta AM, Kirsch RF, Perreault EJ (2000) A robotic manipulator for the characterization of two-dimensional dynamic stiffness using stochastic displacement perturbations. J Neurosci Methods 102:177–186

Agarwal GC, Gottlieb GL (1977) Compliance of the human ankle joint. J Biomech Eng 99:166–170

Akazawa K, Milner TE, Stein RB (1983) Modulation of reflex EMG and stiffness in response to stretch of human finger muscle. J Neurophysiol 49:16–27

Bendat JS, Piersol AG (1986) Random data: analysis and measurement procedures. Wiley, New York

Bennett DJ (1994) Stretch reflex responses in the human elbow joint during a voluntary movement. J Physiol 474:339–351

Bizzi E, Abend W (eds) (1983) Posture control and trajectory formation in single- and multi-joint movements. Raven Press, New York

Cannon SC, Zahalak GI (1982) The mechanical behavior of active human skeletal muscle in small oscillations. J Biomech 15: 111–121

Colgate JE, Hogan N (1988) Robust control of dynamically interacting systems. Int J Control 48:65–88

De Serres J, Milner TE (1991) Wrist muscle activation patterns and stiffness associated with stable and unstable mechanical loads. Exp Brain Res 86:451–458

Dolan JM, Friedman MB, Nagurka ML (1993) Dynamic and loaded impedance components in the maintenance of human arm posture. IEEE Trans Systems Man Cybern 23:698–709

Feldman AG (1966) Functional tuning of nervous system with control of movement or maintenance of a steady posture – III. Mechanographic analysis of the execution by man of the simplest motor tasks. Biofizika 11:667–675

Flash T, Mussa-Ivaldi FA (1990) Human arm stiffness characteristics during the maintenance of posture. Exp Brain Res 82:315–326

Gomi H, Kawato M (1997) Human arm stiffness and equilibrium-point trajectory during multi-joint movement. Biol Cybern 76: 163–171

Gomi H, Osu R (1998) Task-dependent viscoelasticity of human multijoint arm and its spatial characteristics for interaction with environments. J Neurosci 18:8965–8978

Hoffer JA, Andreassen S (1981) Regulation of soleus muscle stiffness in premammillary cats: intrinsic and reflex components. J Neurophysiol 45:267–285

Hogan N (1985) The mechanics of multi-joint posture and movement control. Biol Cybern 52:315–331
Hunter IW, Kearney RE (1982) Dynamics of human ankle stiffness: variation with mean ankle torque. J Biomech 15:747–752
Kearney RE, Stein RB, Parameswaran L (1997) Identification of intrinsic and reflex contributions to human ankle stiffness dynamics. IEEE Trans Biomed Eng 44:493–504
Kirsch RF, Rymer WZ (1992) Neural compensation for fatigue-induced changes in muscle stiffness during perturbations of elbow angle in human. J Neurophysiol 68:449–470
Kirsch RF, Boskov D, Rymer WZ (1994) Muscle stiffness during transient and continuous movements of cat muscle: perturbation characteristics and physiological relevance. IEEE Trans Biomed Eng 41:758–770
Lacquaniti F, Licata F, Soechting JF (1982) The mechanical behavior of the human forearm in response to transient perturbations. Biol Cybern 44:35–46
Lacquaniti F, Carrozzo M, Borghese NA (1993) Time-varying mechanical behavior of multijointed arm in man. J Neurophysiol 69:1443–1463
Mann KA, Werner FW, Palmer AK (1989) Frequency spectrum analysis of wrist motion for activities of daily living. J Orthop Res 7:304–306
Marmarelis PZ, Marmarelis VZ (1978) Analysis of physiological systems. Plenum Press, New York
McIntyre J, Mussa-Ivaldi FA, Bizzi E (1996) The control of stable arm postures in the multi-joint arm. Exp Brain Res 110:248–264
Mussa-Ivaldi FA, Hogan N, Bizzi E (1985) Neural, mechanical, and geometric factors subserving arm posture in humans. J Neurosci 5:2732–2743
Perreault EJ, Kirsch RF, Acosta AM (1999) Multiple-input, multiple-output system identification for the characterization of limb stiffness dynamics. Biol Cybern 80:327–337
Strang G (1998) Introduction to linear algebra. Wellesley-Cambridge Press, Wellesley
Stroeve S (1999) Impedance characteristics of a neuromusculoskeletal model of the human arm I. Posture control. Biol Cybern 81:475–494
Tax AA, Denier van der Gon JJ, Erkelens CJ (1990) Differences in coordination of elbow flexor muscles in force tasks and in movement tasks. Exp Brain Res 81:567–572
Tsuji T, Morasso PG, Goto K, Ito K (1995) Hand impedance characteristics during maintained posture. Biol Cybern 72: 475–485
van Bolhuis BM, Gielen CC (1997) The relative activation of elbow-flexor muscles in isometric flexion and in flexion/extension movements. J Biomech 30:803–811
van der Helm FC, Veeger HE, Pronk GMV, Van der Woude LH, Rozendal RH (1992) Geometry parameters for musculoskeletal modeling of the shoulder system. J Biomech 25:129–144
van Groeningen CJ, Erkelens CJ (1994) Task-dependent differences between mono- and bi-articular heads of the triceps brachii muscle. Exp Brain Res 100:345–352
Weiss PL, Hunter IW, Kearney RE (1988) Human ankle joint stiffness over the full range of muscle activation levels. J Biomech 21:539–544
Zhang L-Q, Rymer WZ (1997) Simultaneous and nonlinear identification of mechanical and reflex properties of human elbow joint muscles. IEEE Trans Biomed Eng 44:1192–1209